Industrial Crops & Products 180 (2022) 114708

Contents lists available at ScienceDirect

Industrial Crops & Products

journal homepage: www.elsevier.com/locate/indcrop

When the order matters: Impacts of lignin removal and xylan conformation on the physical structure and enzymatic hydrolysis of sugarcane bagasse

Melissa Cristina do Espirito Santo [a,1], Force Tefo Thema [b,1], Vanessa de Oliveira Arnoldi Pellegrini [a], Aissata Ousmane Kane [a], Francisco Eduardo Gontijo Guimaraes [a], Jefferson G. Filgueiras [c], Etelvino Henrique Novotny [d], Eduardo Ribeiro DeAzevedo [a], Igor Polikarpov [a,*]

[a] São Carlos Institute of Physics, University of São Paulo, Avenida Trabalhador São-carlense, 400, Parque Arnold Schimidt, 13566-590 São Carlos, SP, Brazil
[b] Faculty of Animal and Veterinary Sciences, Botswana University of Agriculture and Natural Resources, P/Bag 0027, Gaborone, Botswana
[c] Institute of Chemistry, Fluminense Federal University, Outeiro de São João Batista, 24020-141 Niterói, RJ, Brazil
[d] Embrapa Soils, Rua Jardim Botânico, 1024, CEP, 22460-000 Rio de Janeiro, RJ, Brazil

ARTICLE INFO

Keywords:
Biomass pretreatment
Xylan conformation
Sugarcane bagasse
Enzymatic hydrolysis, physical structure

ABSTRACT

Dilute acid and alkaline pretreatments are commonly used to fractionate lignocellulosic biomass for its conversion into biofuels and renewable materials. In the current work, we compare the structure and morphology of one and two-step alkaline and acid pretreated sugarcane bagasse (SCB) and differences in their enzymatic hydrolysis rates and yields. We used physical techniques such as nuclear magnetic resonance (NMR) and X-ray diffraction to shed light on physical and morphological changes introduced by the pretreatments in SCB. We also applied solid state NMR procedures which allowed us to separate xylan structural conformations inside pretreated plant biomass samples. Our results reveal that practically all xylan in two-step "alkaline first" (NaOH 1% + H_2SO_4 1%) pretreated samples adopts two-fold ribbon-like conformation, tightly associated with crystalline cellulose. On the contrary, a main part of xylan in the SCB samples after "acid first" (H_2SO_4 1% + NaOH 1%) combined pretreatment has a three-fold screw conformation characteristic of xylan bound to lignin. Modifications in the biomass composition, physical structure and xylan conformation introduced by the alternative pretreatments contribute to the observed differences in the enzymatic hydrolysis rates and yields. These results could be relevant for analysis and optimization of pretreatments and enzymatic hydrolysis of lignocellulosic biomass in general.

1. Introduction

Lignocellulosic biomass is an important feedstock for production of sustainable materials, biofuels and green chemicals (Himmel et al., 2007). The efficient and cost-effective use of waste-based resources for transformation into value-added products is essential for building of bioeconomy (Ragauskas et al., 2006). Plant biomass is composed by three main polymeric components: lignin, cellulose and hemicelluloses that are associated with each other (Fengel and Wegener, 1984). Xylan, which is a major fraction of hemicellulose, adopts a three-fold helical screw conformation in solution and flattens into a two-fold helical screw ribbon-like conformation intimately binding to cellulose microfibrils in the cell wall (Simmons et al., 2016). Multiple layers of xylan in two-fold screw conformation cover cellulose microfibrils, thus protecting them from direct interactions with water or hydrolytic enzymes. On the other hand, xylan in the absence of cellulose assumes three-fold screw conformation (Simmons et al., 2016). It was recently shown that lignin preferentially binds xylans in three-fold helical screw conformation, which is characteristic of xylans not associated with cellulose (Kang et al., 2019).

Fractionation of the biomass into major components and efficient enzymatic saccharification of xylans and glucans are essential

Abbreviations: CrI, crystallinity index; HPLC, high performance liquid chromatography; MCR, Multivariate Curve Resolution; PCA, Principal Component Analysis; SCB, sugarcane bagasse; ssNMR, solid-state nuclear magnetic resonance; XOS, xylooligosaccharides; XRD, X-ray diffraction; ILT, Inverse Laplace Transform.

* Corresponding author at: São Carlos Institute of Physics, University of São Paulo, Avenida Trabalhador São-carlense, 400, Parque Arnold Schimidt, 13566-590 São Carlos, SP, Brazil.
E-mail address: ipolikarpov@ifsc.usp.br (I. Polikarpov).

[1] These authors contributed equally to this work

https://doi.org/10.1016/j.indcrop.2022.114708
Received 8 September 2021; Received in revised form 17 February 2022; Accepted 19 February 2022
Available online 7 March 2022

prerequisites in its use for production of energy and bioproducts (Himmel et al., 2007; Ragauskas et al., 2006; Suckling et al., 2017; Chabbert et al., 2018). Pretreatment process is one of the most important steps to separate the biopolymers and improve enzymatic digestibility (Silveira et al., 2015; Lloyd et al., 2017; Singh et al., 2016; Mosier et al., 2005). Dilute acid and alkali pretreatment were extensively investigated in several studies on different types of biomasses (Silveira et al., 2015; Mosier et al., 2005; Park & Kim, 2012; Kim et al., 2016). Dilute sulfuric acid pretreatment has been classified as an excellent cost-effective pretreatment technology which might cause significant hydrolysis and solubilization of hemicellulose (Silveira et al., 2015; Lloyd et al., 2017; Mosier et al., 2005). On the other hand, sodium hydroxide is a strong base catalyst, applied in biomass pretreatment for a long time due to its effectiveness as evidenced by higher enzyme hydrolysis yields when compared with other alkaline pretreatments (Park and Kim, 2012; Kim et al., 2016). Alkaline pretreatment leads to degradation and solubilization of lignin fragments, thus causing delignification of the remaining solid fraction (Park and Kim, 2012; Kim et al., 2016). Extensive research of pretreatment technologies has been conducted aiming at optimization of the parameters to improve substrate digestibility using different chemical solvents, such as alkali and acids or their combinations in two-step pretreatments (Silveira et al., 2015; Lloyd et al., 2017; Mosier et al., 2005; Park and Kim, 2012; Kim et al., 2016). Several studies applied acid followed by alkali in combined two-step pretreatments to isolate cellulose and to improve enzymatic hydrolysis using cellulases (Rezende et al., 2011; Maeda et al., 2011). However, the effects of such pretreatments on the structure of biomass and efficiency of enzymatic hydrolysis remain be understood. Specifically, apparent severity of the combined pretreatments should not be affected by the order of the applied pretreatments (alkaline-acid or acid-alkaline), provided that their experimental conditions remain unchanged. Although mathematically obvious, this seemingly straightforward conclusion could be challenged by a complexity and irreversibility of the studied processes.

In this work, we investigated the effects of the order in two-steps pretreatments, starting with alkaline followed by acid pretreatments as well as the opposite, using dilute acid and alkaline pretreatments, on the structure and morphology of the sugarcane bagasse with a wide array of physical techniques including solid state nuclear magnetic resonance (ssNMR), X-ray diffraction (XRD) and confocal laser scanning microscopy (CLSM). Details of the structure and chemical composition of the plant biomass after each applied pretreatment condition were correlated with the changes observed in the enzymatic hydrolysis yields. Our results show that the order of pretreatments has a strong effect on the structure of lignocellulosic biomass as well as the rates of its enzymatic hydrolysis. We demonstrate that "acid first" combined pretreatment removes much larger fraction of xylan in strongly associated with cellulose two-fold ribbon-like conformation, as compared to "alkali first" combined pretreatment, mostly leaving behind xylan in three-fold conformation, characteristic of xylan bound to lignin. This could have important impacts on the efficiencies and rates of lignocellulosic biomass enzymatic hydrolysis.

2. Material and methods

2.1. Feedstock and the enzyme preparation

Sugarcane bagasse used in this study was collected at Raízen sugarcane mill (Costa Pinto, Piracicaba, SP, Brazil). The unwashed material was dried at 40 ºC and its moisture content was measured. The biomass was then stored in plastic containers at room temperature until further use. Commercial cellulase mixture Accelerase® 1500 (14 mg protein/mL enzyme preparation) used for enzymatic hydrolysis reactions was generously provided by Genencor (Rochester, NY, USA). Accellerase® 1500 enzyme complex is produced with a genetically modified *Trichoderma reesei* strain and contains multiple enzymatic activities, including exo- and endoglucanases, hemicellulases, and beta-glucosidases, among others (Anon, 2021).

According to published data, Avicelase, CMCase, cellobiase and xylanase activities of Accelerase 1500 are 0.77 ± 0.02, 56 ± 3.0, 5.6 ± 0.3 and 21 ± 1.0 (U/mg-protein) of enzyme preparation (Kawai et al., 2012). Alternatively determined cellobiohydrolase, endoglucanase, beta-glucosidase and xylanase activities of Accelerase 1500 are 0.31 ± 0.02, 14.9 ± 0.1, 1.48 ± 3.0 and 6.25 ± 0.08 (U/mg-protein) with overall FPU activity of 0.45 U/mg-protein (Yang et al., 2017).

2.2. Conditions of pretreatment

Four different pretreatments were conducted: 1) alkaline pretreatment, 2) acid pretreatment, 3) alkali pretreatment followed by acid pretreatment (alkaline first) and 4) acid pretreatment followed alkaline pretreatment (acid first). The conditions of the acid and alkaline pretreatments were maintained the same in each set of the pretreatments tested.

The pretreatment conditions were based on Rezende et al. Rezende et al. (2011) and Maeda et al. Maeda et al. (2011). For acid pretreatment the reaction was maintained in an autoclave at additional pressure of 1.05 bar and a 1:10 solid to liquid ratio (grams of bagasse/mL of solution) using diluted sulfuric acid (1% v/v in water) for 40 min at 120 °C. The solid fraction of pretreated bagasse was separated from the hydrolysate by filtration. The applied alkaline pretreatment was performed using these same parameters, but diluted acid was substituted by diluted sodium hydroxide (1% w/v) (Rezende et al., 2011; Maeda et al., 2011). The two other pretreatments were a sequential combination of acid and alkaline pretreatments. Pretreatment #4 started with 1% H_2SO_4 and after reaction in the autoclave, the sample was allowed to cool down to room temperature, then was washed until pH 7 and dried, prior to being submitted to the second sequential pretreatment step using 1% NaOH (herein denoted as H_2SO_4 1% + NaOH 1% or "acid first" pretreatment). Pretreatment #3 was opposite in the order of pretreatments, starting with 1% NaOH pretreatment and then submitting the pretreated bagasse to dilute acid pretreatment with 1% H_2SO_4 (herein termed NaOH 1% + H_2SO_4 1% or "alkali first" pretreatment). The cooled alkaline pretreated SCB sample was washed until pH 7 was reached, before proceeding with the acid pretreatment.

2.3. Severity Factor

The severity factor, calculated according Overend and Chornet (Overend and Chornet, 1987), was based on the following Eq. (1):

$$\log R_0 = \log\left[\sum_{i=1}^{n} t_i . exp\left(\frac{T_i - T_b}{\omega}\right)\right] \quad (1)$$

Eq. (1) combines the experimental effects of temperature (T; in °C) and reaction time (t; in minutes) where T_b= 100 is the reference temperature (ºC). The fitted value (14.75) of the arbitrary constant ω, is based on the activation energy when assuming pseudo first order kinetics (Overend and Chornet, 1987; Carvalheiro et al., 2009). Although the arbitrary constant ω was established for the wheat straw, it is being widely used for sugarcane bagasse (da Cruz et al., 2012; Ilanidis et al., 2021; Espirito Santo et al., 2020) and other types of plant biomass.

2.4. Chemical composition analysis

The chemical compositions of plant biomass samples were determined using the protocols established by Rocha and coworkers (Rocha et al., 2011) with some adaptations described in (Santo et al., 2018). First, the solid samples were milled using a knife mill with 20-mesh interior sieve. The moisture contents of all materials were measured with Shimadzu MOC120H model (Kyoto, Japan) heating balance and used to calculate their dry weights (Santo et al., 2018).

Next, all fractions that were subjected to concentrated acid

hydrolysis (H_2SO_4 72%) and their monomeric components such as sugars (glucose, xylose, arabinose) and organic acids (acetic acid, formic acid) were quantified using high performance liquid chromatography (HPLC) (Rocha et al., 2011; Santo et al., 2018). The chromatographic system (Shimadzu, LC-20AT) was equipped with a refractive index (RI) detector (Waters 2414, USA) and an Aminex HPX-87 H (Bio-Rad, Richmond, CA) column maintained at 65 °C in an eluent flow at 0.6 mL/min with 5 mM sulfuric acid (Santo et al., 2018).

To determine chemical compositions of the sugarcane bagasse samples, their main fractions, such as cellulose, hemicellulose, lignin, extractives and ashes were quantified and the mass closures were computed (Coletta et al., 2013; Sun and Cheng, 2005). Amount of cellulose was calculated by summing up glucose and cellobiose. Amount of hemicellulose was computed by considering amounts of xylose, arabinose and acetic acid. The total lignin amount included soluble and insoluble lignin fractions (Santo et al., 2018). Finally, ash was determined as the remaining inorganic fraction after the bagasse samples were carbonized in a muffle, with heating ramps of 1 h at 200 ºC, 1 h at 400 ºC and 2 h at 800 ºC (Santo et al., 2018). All experiments were conducted in triplicates.

2.5. Enzymatic hydrolysis

Batch enzymatic hydrolysis was carried out in 50 mM sodium citrate buffer (pH 5.0) supplemented with 5 mg of enzyme Accellerase 1500 (Genencor, Rochester, NY, USA) loading per gram of biomass in a shaker at constant agitation (150 rpm) and temperature (50 °C) for 72 h. This enzymatic load corresponds to approximately 1.5 U, 74.5 U, 7.4 U and 31.25 U of cellobiohydrolase, endoglucanase, beta-glucosidase and xylanase activities with overall filter-paper activity of 2.25 FPU (Kawai et al., 2012). The total solids concentration used in the reactions were 5% (w/v). To follow a release of soluble sugars, each 24 h the aliquots of supernatant were collected from the enzymatic hydrolysis reaction flasks for HPLC analyses. Prior to application into HPLC system, the samples were heated at 100 ºC for 10 min to stop the enzymatic activities, centrifuged and filtered. All experiments were done in triplicates.

Both glucan and xylan conversion during enzymatic hydrolysis reactions were calculated based on sugar concentrations in the hydrolysates using Shimadzu LC-20AT chromatographic system equipped with RI detector (Waters 2414, USA) and an Aminex HPX-87 H column (Bio-Rad, Richmond, CA) kept at 65 °C. An eluent flow of 5 mM sulfuric acid at 0.6 mL/min was applied.

The enzymatic hydrolysis efficiencies of glucan (EHG) and xylan (EHX) conversions were calculated according to the following equations

$$EHX(\%) = \frac{c_{glucose}}{c_{substrate} \times cellulose \quad content \quad in \quad substrate} \times 0.9 \times 100\%$$

and

$$EHX(\%) = \frac{c_{xylose}}{c_{substrate} \times xylan \quad content \quad in \quad substrate} \times 0.88 \times 100\%$$

where $c_{substrate}$ was the substrate loading (g) and $c_{glucose}$ and c_{xylose} were amounts of glucose and xylose in the enzymatic hydrolysates (g).

2.6. X-Ray diffraction analyses

Previously dried samples were subjected to X-ray diffraction (XRD) analyses conducted at a room temperature using monochromatic CuKα radiation (1.54 Å) on Rigaku Rotaflex X-ray diffractometer (RU200B model; Tokyo, Japan). The X-ray diffraction equipment was set at 40 kV and 15 mA. 2θ scans were measured from 5° to 50° in 0.05° steps with an X-ray exposure of 15 s per step. All measurements were done in duplicates.

Segal empirical method (Segal et al., 1959) was applied to derive the crystallinity indices (CrIs), whereas average crystallite sizes were calculated using the Scherrer equation (Scherrer, 1912; Monshi et al., 2012).

2.7. Low-field nuclear magnetic resonance (NMR)

All samples were first dried at 80 ℃ under an 800 mmHg vacuum for 5 h. After this procedure all the samples were soaked with ultrapure water (Millipore Inc.) overnight. The excess of water was removed by centrifuge filtration (Corning® Costar® Spin-X, 0.45 μm, nylon membrane) with a relative centrifuge force of 100 g for 1 min. All measurements were performed on a Bruker Minispec MQ-20 spectrometer, with a 0.5 T magnetic field (^{1}H Larmor frequency of 20 MHz), by using a CPMG (Carr-Purcell-Meiboom-Gill) sequence, with the acquisition of 35,000 echoes. Echo times of 70 μs and recycle delays of 10 s were used. To obtain the T_2 distributions for each sample, a numerical Inverse Laplace Transform (ILT) procedure (ILT) was applied (Borgia et al., 1998). The contribution of each interstitial scale of the biomass was obtained by deconvoluting T_2 distributions with log-gaussian functions. All experiments were carried out in duplicate, and the ILT was carried out on the CPMG decay given by a mean of the normalized data from these two experiments.

When a fluid is confined inside a pore, the interactions between the pore surface and the ^{1}H nuclear spins of the fluid molecules imply on a reduction of the observed transverse relaxation rates, T_2. This effect is directly dependent on the pore size and the T_2 distribution of a fluid confined on a given porous system reflects its pore size distribution media in a qualitative fashion. On the fast diffusion limit, the relation between T_2 and the pore size is given (Capitani et al., 2012)

$$1/T_2 = \rho \quad (S/V) = 2\rho/r, \tag{2}$$

where ρ is the surface relaxivity, which depends on the porous media and is usually unknown, and S and V are the pore surface area and its volume, respectively. The distribution of pore sizes and differences in the fluid mobility within the pores both impact the T_2 distributions.

2.8. ^{13}C Solid-state NMR spectroscopy

Solid-state NMR spectroscopy experiments were performed with Varian Unit Inova spectrometer operating at frequencies of 100.5 MHz and 400.0 MHz for ^{13}C and ^{1}H, respectively. A 5 mm double resonance magic angle spinning probe with a frequency stability superior to 2 Hz was used. Ramped cross-polarization under magic angle spinning (^{13}C CPMAS) with RF amplitude varying between 80% and 100% during 1 ms of contact time was performed as excitation method. Magic angle spinning of 10 kHz, high power dipolar decoupling of 70 kHz, ^{13}C and ^{1}H 90° pulse durations of 3.5 and 4.0 μs, respectively, were typically used. All ssNMR measurements were performed using 2 s recycle delays.

2.9. Multivariate Curve Resolution (MCR) analysis of Torchia T_1 experiments

We used a multivariate mathematical procedure for the separation of spectral components with different T_1 in the solid-state NMR data. A Multivariate Curve Resolution (MCR) procedure (Novotny et al., 2009; Espirito Santo et al., 2019) was performed using the software The Unscrambler® v10.4.1 (CAMO Software AS). MCR allows determination of a number of components co-existing in a chemical system allowing for extraction of the pure spectra of the components (qualitative analysis) as well as the concentration profiles of each component (quantitative analysis), as long as they have different variability as a function of the sources of variation present in the data matrix. This is achieved by applying a standard Principal Component Analysis (PCA) to estimate the probable number of components in the mixture and then calculating a rotation of the PCs without the orthonormality constraints, but allying new constraints: non-negative concentrations and non-negative spectra.

Here we analyze the variability due to the modulation of the NMR spectra induced by a pulse sequence known as Torchia T_1 (or CPT_1) (Torchia, 1978). In brief, this pulse sequence modulates the CPMAS spectrum by an exponential decay of the type $e^{-\frac{\tau}{T_1}}$ where τ, so-called filter time, is an experimentally defined time period. Thus, for the same τ, signals with shorter ^{13}C T_1 relaxation time are more strongly attenuated. Since in this particular case decays of the intensities were themselves the relevant variations, the usual spectra normalizations (e.g. maximum area or unit vector normalization of each spectrum) were not very useful. Instead, the average decay of each sample (decay of the full spectra area as a function of τ) was fitted by a mono-exponential function and the I_0 (intensity at $\tau = 0$) was used to normalize each individual spectrum. The full data set was composed by 30 spectra, i. e. three pretreatments (NaOH 1%; NaOH 1% + H_2SO_4 1% and H_2SO_4 1% + NaOH 1%) and Torchia T_1 spectra acquired with τ = 0.1 s, 0.5 s, 1.0 s, 1.5 s, 2.0 s, 2.5 s, 3.0 s, 4.0 s, 5.0 s, 8.0 s for each sample. It is important to mention that we did not include the raw SCB and the sample pretreated only with diluted H2SO4 in the MCR analysis because the presence of strong lignin signals would overwhelm the more subtle differences between the sample submitted to the combined pre-treatments, which were the main focus of our study.

3. Results and Discussion

3.1. Changes in chemical composition of the samples caused by pretreatments

The chemical composition quantification and the compositional changes of sugarcane bagasse caused by the pretreatments are summarized in Table 1. Note that the pretreatments affected mainly hemicellulose and lignin, but their degradation varied significantly depending on the pretreatment conditions. The dilute alkaline (NaOH 1%) pretreatment led to lignin solubilization, caused by the cleavage of hydrolysable linkages such as α- and β- aryl ether bonds. Alkyl aryl linkages in lignin are readily cleaved under alkaline conditions such as the ones maintained during the NaOH pretreatment. Sodium hydroxide is dissociated into hydroxide ion (OH^-) and sodium ion (Na^+) and the hydroxide ion acts as a catalyst in the hydrolytic reactions (Park and Kim, 2012; Kim et al., 2016). Further, according to previous studies (Park and Kim, 2012; Kim et al., 2016), sodium hydroxide effectively attacks the linkages between lignin and hemicellulose. Specifically, it cleaves the ether and ester bonds, as well as the ester and carbon-to-carbon (C–C) bonds in lignin molecules (Park and Kim, 2012; Kim et al., 2016). The main reaction that occurs during the acid pretreatment is the hydrolysis of hemicellulose, making the cellulose more accessible to the enzymes (Silveira et al., 2015; Sun and Cheng, 2005). During dilute acid pretreatments, partially solubilized lignin might condensate and precipitate at the surface of the biomass, particularly at the high acid concentrations (Silveira et al., 2015; Sun and Cheng, 2005).

Our analyses of the dilute acid pretreated solids did not reveal significant removal of lignin, but the depolymerization of hemicellulose was clearly evident (Table 1). A combination of acid and alkaline pretreatments could remove most of the non-cellulosic materials, making cellulose even more accessible (Park and Kim, 2012; Maeda et al., 2011). Sulfuric acid and sodium hydroxide have been studied for effective hemicellulose and lignin removal, respectively (Park and Kim, 2012; Maeda et al., 2011). For example, Rezende and co-workers (Park and Kim, 2012) removed most of the hemicellulose fraction in the first stage of combined pretreatment using dilute sulfuric acid and solubilized most of the remaining lignin in the second, alkaline stage, using sodium hydroxide. The combination of pretreatments resulted in a high cellulose concentration and positively impacted the enzymatic hydrolysis yields (Park and Kim, 2012).

As expected (Park and Kim, 2012), our analyses show that acid and alkaline pretreatments lead to removal of predominantly hemicellulose and lignin from pretreated biomass, respectively (Table 1). Both combined pretreatments further contributed to the removal of none-cellulose fractions from the pretreated biomass. However, extend of lignin removal was impacted by the order of applied pretreatments. When the first pretreatment step was alkaline pretreatment and the second step was dilute acid pretreatment ("alkaline first"), the resulting combined pretreatment was more efficient in lignin removal as compared to the pretreatment in which the opposite order of single pretreatment steps was applied ("acid first" pretreatment). Hemicellulose concentration in the "alkaline first" and "acid first" pretreated biomass samples was about the same, but glucan content of the latter sample was somewhat smaller (Table 1).

It is important to stress that all the pretreatment parameters were maintained the same, resulting in the equal combined severity of the applied two-step pretreatments. According to Eq. 1, the severity factor combines the experimental effects of temperature and reaction time. The only difference in this study was the order of applied pretreatments (acid first or alkaline first). There is, of course, a noticeable difference in the combined severity between single (1.7) vs. double (Ragauskas et al., 2006) pretreatment methods (Table 1). Therefore, one would expect to see considerable difference in morphology and efficiency of enzymatic hydrolysis of SCB samples subjected to single and double pretreatments.

Thus, we applied a range of physical techniques to investigate the differences in structure and morphology of the biomass samples imprinted by the four different pretreatment strategies.

3.2. Low field Nuclear Magnetic Resonance (NMR) characterization

Pretreatments are applied to cause changes in the chemical and physical properties of plant biomass, which accompany preferential degradation and solubilization of particular biopolymers (Silveira et al., 2015; Park and Kim, 2012; Kim et al., 2016). Such changes might impact porosity and crystallinity of the remaining material.

NMR relaxometry experiments revealed the presence of interstitial spaces (usually referred as pores) with three different length scales in the SCB samples used in the present study. Because the NMR signal is all related to water molecules inside these spaces, what is detected in such experiments is water filled pores within the sample. Despite the actual sizes of the pores are difficult to quantify precisely, typical dimensions of water accessible interstitial spaces in the SCB ranges from ~ 100 nm to ~ 10 μm. Thus, typical pore sizes in SCB samples as seen by NMR relaxometry might be associated to interstitial spaces at the fibril

Table 1
Chemical composition of sugarcane bagasse in different conditions. Recovery of solids after NaOH 1%, H_2SO_4 1%, H_2SO_4 1% + NaOH 1% and NaOH 1% + H_2SO_4 1% were 66%, 64%, 48% and 50%, respectively.

	Cellulose	Hemicellulose	Lignin	Ash	Total	Severity Factor
Raw bagasse	38.1 ± 0.2	25.8 ± 0.1	26.7 ± 0.2	1.7 ± 0.2	100 ± 0.7[a]	
NaOH 1%	52.1 ± 0.2	26.1 ± 0.1	12 ± 1	1.3 ± 0.2	91 ± 2	1.7
H_2SO_4 1%	56 ± 1	9.0 ± 0.1	28.0 ± 0.9	2.2 ± 0.2	95 ± 3	1.7
H_2SO_4 1% + NaOH 1%	63.5 ± 0.5	10.9 ± 0.1	16.8 ± 0.8	0.8 ± 0.2	92 ± 2	2.0
NaOH 1% + H_2SO_4 1%	73.6 ± 0.1	12.1 ± 0.7	13 ± 2	0.7 ± 0.2	99 ± 3	2.0

[a] Extractives = 7.7% in the raw bagasse samples. No extractives were detected in the pretreated samples.

surfaces (shortest T_2 values, about 1 ms), within the lignin-hemicellulose matrix on the surface of the fibers (tens of milliseconds) and luminal pores or spaces between the fibers (hundreds of milliseconds) (Tsuchida et al., 2014; Meng and Ragauskas, 2014). Thus, a T_2 distribution curve measured in such experiments can be deconvoluted in three main components, each one associated to the water molecules inside the corresponding interstitial volume. Thus, the relative proportion of waters inside each kind of interstitial space is obtained by comparison of the relative area of the respective component in the T_2 distribution curve, which is obtained by deconvolution of the curves using log-gaussian functions. We will refer to that as relative % of water inside each kind of interstitial space.

Concerning the interstitial dimensions, there is a direct relation between the pore size (or the inverse of the specific surface area) and the T_2 values. Thus, the center of each component of the measured T_2 distribution curve is proportional to the average size of the pores associated to that component. However, to precisely obtain the average pore sizes one need to know the proportional constant, called the surface relativity constant ρ (see Eq. 2). Since the surface relativities for the SCB structures are unknown, this impedes us to precisely estimate the actual pore sizes for the interstitial observed scales. Other methods, such as BET can provide an estimation of the pore sizes. However, the length scale accessible by BET experiments (~1 to ~100 nm; (Brewer et al., 2014), are shorter and not compatible with the length scale observed in NMR relaxometry measurements (~ 100 nm to ~10 μm). Furthermore, the use of gas physisorption methods, or even mercury porosimetry which length scale is compatible with NMR relaxometry, in biological materials can be problematic (Sigmund et al., 2017). Furthermore, the physisorption is strongly influenced by degassing temperature that can have impacts on the structure and composition of the samples. On the contrary, NMR relaxometry deals with water filled pores providing information on what is sometimes called "wetted specific surface area" (Takai-Yamashita et al., 2020). Thus, although one does not obtain specific pore sizes, but considering the typical dimensions of the enzymes and the fact that enzymatic hydrolysis occurs in water-based solutions, the length scales and the % of water inside interstitial spaces in the lignin-hemicellulose matrix, as probed by NMR relaxometry, seems to be particularly appropriate to correlate with the enzymatic hydrolysis yields.

Thus, by measuring the T_2 distributions for samples which underwent different biochemical processes, it is possible to assess how the microstructure of the biomass is modified at different length scales.

As described in the experimental section, in order to remove bulk water, expected as a component with average T_2 of seconds, we centrifuge the wet samples until this component is not observed. This provides a consistent reproducibility of the measured T_2 distributions, but precludes the precisely control the absolute amount of mass and water in each measurement. Thus, we were only able to assess a relative proportion of water (% of the total absorbed water) within each microstructure component of the pretreated SCB samples, given by the respective relative area on the distributions (Fig. 1). For all samples, the relative area of the smallest component, related to pores at fibril surfaces, was not significant in comparison to the other two components. Moreover, these small components showed themselves particularly sensitive to the regularization parameter of the ILT procedure (Borgia et al., 1998), and as such we assumed that the volumes attributed to these components are too small to be reliably measured and therefore, they were not considered during further data analyses.

As a general trend, we observe that all the pretreatments increased the relative areas related to the largest pore scale in comparison to the raw SCB sample used as a control, thus indicating that the removal of hemicellulose and lignin by the pretreatments results in an increase of % of water in the larger pores. Of note, combined "alkali first" pretreatment rendered considerably different samples as compared to "acid fist" pretreatment (Fig. 1). All % of water in the different interstitial scales obtained from the deconvolutions are shown in Table 2. Comparing the

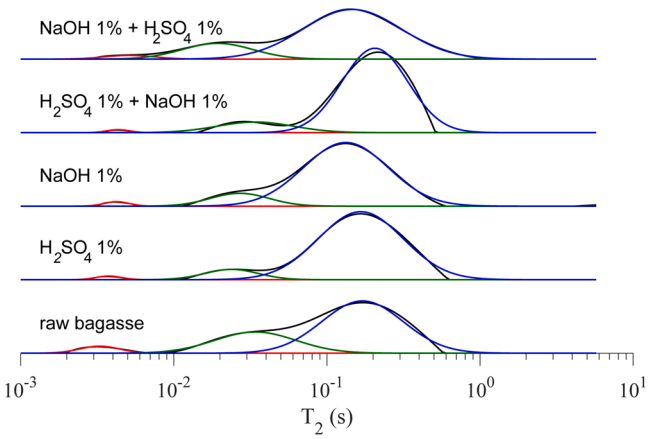

Fig. 1. T_2 distributions for all samples. The distributions are represented by the black solid lines, whereas the components associated to each interstitial scale are shown in red (fibril surfaces), green (inter fibers) and blue (lumens).

Table 2
Relative water accessible areas for five studied SCB types. The values are given in fractions of unity.

Sample	Inner-microfiber	Cell wall	Lumen
Raw bagasse	0.04 ± 0.01	0.28 ± 0.02	0.68 ± 0.02
H_2SO_4 1%	0.01 ± 0.01	0.09 ± 0.01	0.90 ± 0.01
NaOH 1%	0.02 ± 0.01	0.12 ± 0.01	0.86 ± 0.01
H_2SO_4 1% + NaOH 1%	0.01 ± 0.01	0.13 ± 0.02	0.86 ± 0.02
NaOH 1% + H_2SO_4 1%	0.03 ± 0.01	0.18 ± 0.01	0.79 ± 0.01

samples submitted to the combined pretreatment, the % of water in the smaller interstitial scales are significantly higher in the "alkali first" samples. This suggests the absorption of water in the more internal spaces of the biomass was higher for "alkali first" than for "acid first" pretreated samples.

The variations for the central T_2 values of each component in the T_2 distributions in Fig. 1 are a combined effect of modifications both in the pore sizes and the surface relaxivity of the pores, since the pretreatments may modify an affinity of the pore surfaces to the water molecules.

3.3. X-Ray diffraction analyses

It is known that crystallinity might have important effects on the efficiency of enzymatic hydrolysis and could be significantly affected by the lignocellulosic biomass pretreatments (Santo et al., 2018; Park et al., 2010). With this in mind, we determined crystallinity indices (CrIs) of raw and pretreated biomass samples using X-ray diffraction measurements (Table 3).

Analysis of the crystallinities (Table 3) and chemical composition of SCB samples (Table 1) shows that the changes in SCB crystallinity was primarily due to removal of lignin, hemicellulose and amorphous regions of cellulose, caused by pretreatments (Rezende et al., 2011).

CrIs estimates based on the Segal equation (Table 3) agree well with the decrease in lignin and hemicellulose contents of the pretreated samples (Table 1). Lower CrI values were observed for H_2SO_4 1% and

Table 3
Crystallinity index and cellulose crystallite size in sugarcane bagasse samples.

Samples	CrI (%)	Average crystallite size (nm)
Raw bagasse	38.3 ± 0.5	3.3 ± 0.1
NaOH 1%	48 ± 2	3.9 ± 0.2
H_2SO_4 1%	40 ± 3	3.8 ± 0.2
H_2SO_4 1% + NaOH 1%	46.7 ± 0.1	3.7 ± 0.1
NaOH 1% + H_2SO_4 1%	48 ± 2	3.9 ± 0.2

raw bagasse samples is consistent with their higher lignin content as compared with the other pretreated samples.

According to Driemeier and co-workers (Driemeier et al., 2015) hemicellulose and lignin removal promotes direct interfacing between cellulose crystallites, enabling co-crystallization that results in larger crystallites. This notion is consistent with our results (Table 2), which show that all the applied pretreatments resulted in larger crystallites.

3.4. ^{13}C solid state NMR Spectroscopy

To evaluate possible differences in the sample composition and/or cellulose microstructure resulting from the pretreatments we applied ^{13}C solid state NMR spectroscopy analyses. The ^{13}C-CPMAS spectra of the pretreated SCB samples are shown in Fig. 2 A.

Chemical shifts were assigned as described previously (Rezende et al., 2011). The spectra of raw SCB and dilute acid pretreated SCB samples can be found elsewhere (Rezende et al., 2011; Santo et al., 2018; Novotny et al., 2009). The absence of signals at ~ 23 ppm (methyl groups) and ~170 ppm (carbonyl/carboxyl) (Fig. 2) suggests that all the pretreatments were effective in reducing the amount of acetylated hemicellulose components to below the noise level of our ssNMR spectra (~2%). The strong decrease of lignin signals (signals within 120 – 180 ppm region are from aromatic components and at 55.6 ppm are from OCH_3 groups) as well as the increase in the resolution of the spectra in the 50–120 ppm region were observed for the samples pretreated with NaOH due to the partial lignin removal. The remaining signals in the aromatic and OCH_3 regions show that a significant portion of the lignin is retained in the samples even after the applied alkaline pretreatment with NaOH, which is consistent with our CLSM results. However, in the 80–92 ppm region the lignin signals are small as compared with the carbohydrate signals (Bernardinelli et al., 2015). Thus, for alkaline pretreated samples this spectral region can be mostly attributed to the C4 carbons of carbohydrates.

For cellulose chains, the split observed for the C4 carbon signal (80–92 ppm) and C6 signal (62–66 ppm) (inset in Fig. 2 A) is attributed to two distinct cellulose environments referred to as domain 1 (signals at ~88 and ~65 ppm ppm), and domain 2 (signals at ~84 ppm and 62 ppm). Previously, domain 1 has been attributed to more ordered cellulose chains in the core of the microfibril, sometimes referred to as crystalline cellulose, while domain 2 was attributed to cellulose chains at the surface of the microfibrils, also referred to as amorphous cellulose (Driemeier et al., 2015; Foston et al., 2011). However, supported by *in muro* ssNMR results (Dupree et al., 2019), a new model for the lignocelulose materials microstructure shows that among the structural features that distinguish the C4 and C6 signals of domains 1 and 2 is the conformation of the carbon 6 hydroxymethyl group, which may change upon the interaction with other cell wall components. It has been demonstrated (Dupree et al., 2019) that for conifer plants the presence of hemicellulose components, particularly xylan and galactoglucomannan, bound to the surface of the microfibril induces domain 1 conformation of some cellulose chains at the surface. Thus, an assignment of domain 1 C4 and C6 signals to internal cellulose and crystalline chains is somewhat misleading. Despite that, changes in the C4 and C6 signals can still be related to the local environment of cellulose in the sense that they distinguish groups of chains with similar conformations in the microfibril.

The inset of Fig. 2 A shows a zoom in the 80–95 ppm and 62–66 ppm spectral regions for the three samples treated with NaOH. Since these samples have similar small amounts of lignin (Table 1), the spectra were normalized by the residual lignin peak at 55.7 ppm. After this normalization, the intensity profiles for alkali pretreated samples (NaOH 1%) and for samples after combined NaOH 1% + H_2SO_4 1% (alkali first) pretreatment are similar between themselves, but different from the intensity profiles of the sample submitted to the combined H_2SO_4 1% + NaOH 1% (acid first) pretreatment. To provide evidence on the origin of this signal, we subtracted the spectra from the samples submitted to

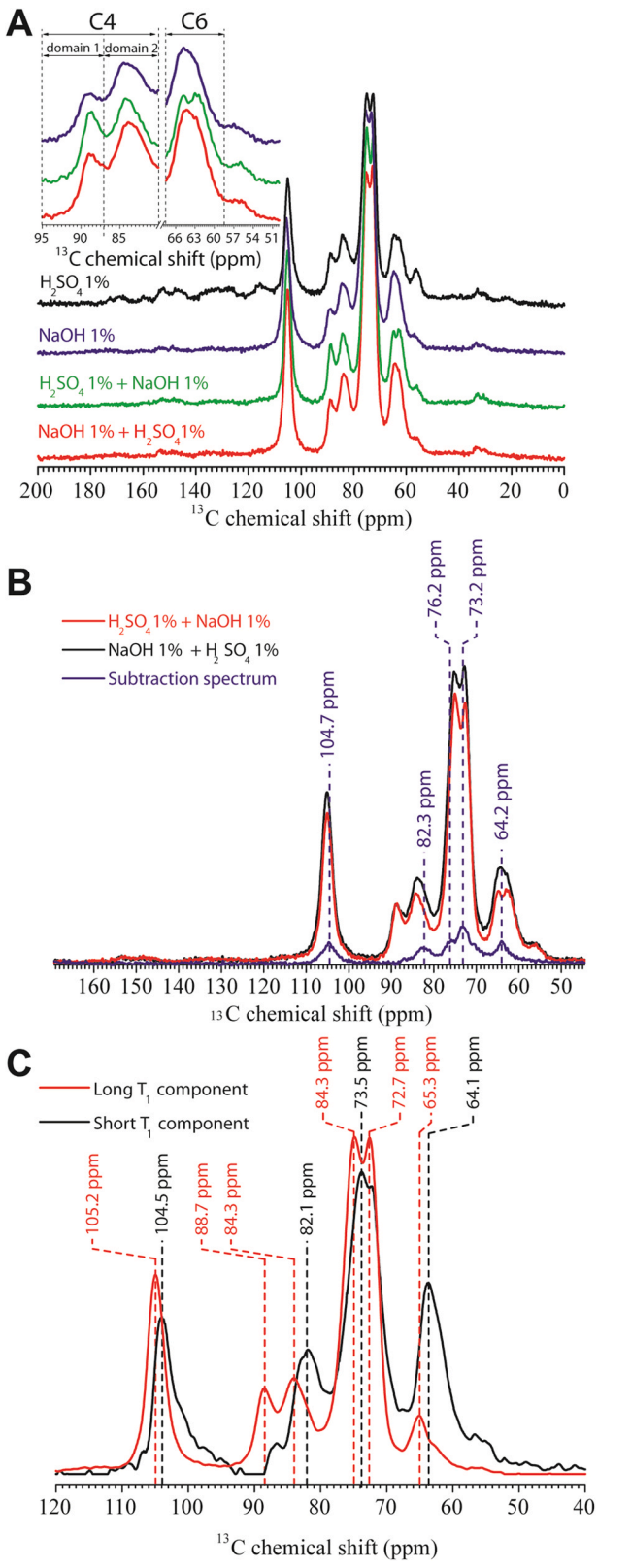

Fig. 2. (A) ^{13}C CPMAS spectra of sugarcane bagasse submitted to different pretreatments as indicated. (B) Comparison between the ^{13}C CPMAS spectra of samples submitted to combined pre-treatments in different orders as well as their subtraction spectra. (C) MCR ^{13}C NMR spectra predicted spectra from the T_1 induced variability provided by the application of the Torchia T_1 pulse sequence. The spectra shown are normalized, but the weight percent of each component in the mixture are shown in Table 4.

both the combined pretreatment with "alkali first" and also "acid first" (Fig. 2B). Remarkably, the difference spectrum clearly shows five different signals at 104.7 ppm, 82.3 ppm, 76.2 ppm, 73.2 ppm and 64.2 ppm, respectively. These signals are usually assigned to hemicellulose carbons (Wickholm et al., 1998; Dick-Pérez et al., 2011). More specifically, the values of the chemical shifts match very well with the chemical shifts expected for xylan in flattened two-fold screw conformation bound to the surface of the cellulose microfibrils as measured in ^{13}C labeled *Arabidopsis* stems using refocused 2D INADEQUATE ^{13}C NMR (105.2 ppm, 82.2 ppm, 75.2 ppm, 72.3 ppm and 64.3 ppm) (Simmons et al., 2016; Dupree et al., 2019; Falcoz-Vigne et al., 2017). In particular, the signals at 105.2 ppm and 82.2 ppm are the fingerprints of xylan in two-fold screw conformation since xylan in three-fold screw conformation and other hemicellulose components are not expected to have peaks at these positions (Simmons et al., 2016). Furthermore, they can be adequately distinguished from the signals expected for cellulose at 84.5 ppm, 65.8 ppm and 62.2 ppm. Furthermore, the absence of CH_3 signal shows that the degree of acetylation of the xylan is rather small, which is known to be a condition for the xylan associated with the surface of cellulose in a two-fold screw conformation (Dupree et al., 2019). Deacetylation of xylan can also be a result of the applied pretreatments with NaOH.

To support the hypothesis that the signals observed in the difference spectrum of Fig. 3B are associated to the two-fold screw conformation of xylan we looked for independent experimental evidence. Thus, we decided to explore the ^{13}C spin-lattice relaxation time (^{13}C T_1) which depends on a fast molecular mobility (in the 100 MHz frequency range) and can be an indicative of the molecules experiencing different intermolecular environments. Therefore, to identify signal components with distinct T_1 relaxation times we acquired the spectra using the ssNMR pulse sequence known as Torchia T_1 (or CPT_1) (33). Simply put, this pulse sequence modulates the CPMAS spectrum by an exponential decay $e^{-\frac{\tau}{T_1}}$ where τ, so-called filter time, is an experimentally defined time period. Thus, for the same τ, signals with shorter ^{13}C T_1 relaxation time will be more attenuated. As an example, a set of Torchia T_1 spectra obtained with different τ for samples submitted to combined pretreatments "alkali first" and "acid first" are shown in Supplementary Figs. S1 A and B. Different decay profiles are observed for distinct chemical shift values, suggesting the existence of molecular domains with distinct relaxation patterns in the samples. For instance, the signals at ~88 ppm show little decay due to the longer T_1 value while the most pronounced decay is observed for the signal associated to the C6 carbon at ~60 to ~65 ppm due to higher mobility of the side chain hydroxymethyl groups. However, it is worth noticing that even for the same carbon types distinct relaxation patterns are observed. This is the case for C4 and C6 carbons for which a change in the line shapes for different τ values suggest the existence of glucopyranose units with different local environments and, consequently, with distinct T_1 relaxation times. Finally, intensity reduction in the spectral regions of 80–84 ppm and 70–80 ppm is different for the samples pretreated with "acid first" or "alkali first". On the other hand, the decay profile observed for the samples pretreated only with NaOH 1% are very similar to that observed for the "alkali first" pretreated samples (not shown).

Given the differences observed in Torchia T_1 profiles we performed a Multivariate Curve Resolution (MCR) procedure seeking to separate spectral components with different T_1 decay profiles (see details in the Material and Methods section). Here, the main source of variation, besides the biomass pre-treatment, was the experimentally induced and controlled T_1 filter time τ, which allowed the separation of compounds with different T_1.

After applying the Principal Component Analysis (PCA) to the full dataset we found that the T_1 induced variation of the spectra could be explained considering a binary mixture with substantially different relaxation times. Using this constraint in the MCR procedure, the predicted spectra of these two components were obtained (indicated as

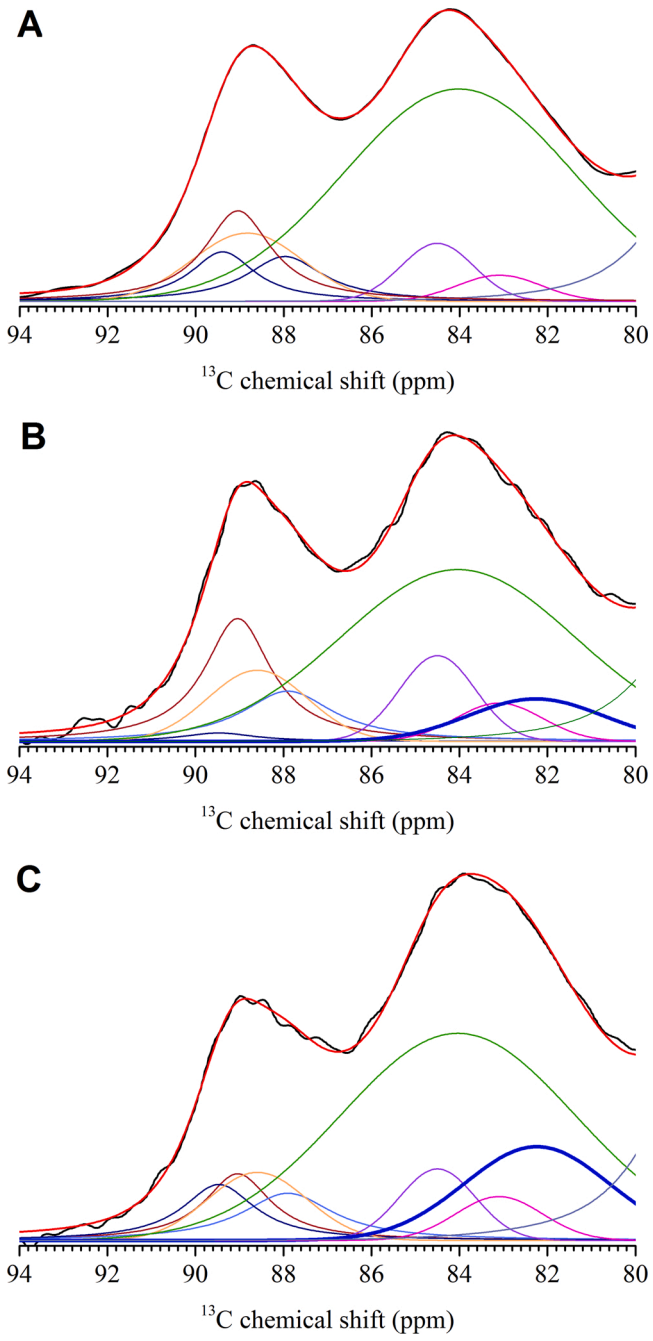

Fig. 3. Deconvolution of the C4 carbon signal based on the existence of 8 cellulose sub-domains as described in the text and a two-fold screw xylan signal at 82.2 ppm. (A) MCR predicted spectra for the long T_1 components. (B) ^{13}C CPMAS spectra from the sample pretreated with H_2SO_4 1%. + NaOH 1% (C) ^{13}C CPMAS spectra from the sample pretreated with NaOH 1% + H_2SO_4 1%. The signal of xylan in two-fold screw conformation is shown as a thicker blue line.

short and long T_1 components in Fig. 2 C). It is remarkable that the spectrum of the short T_1 component has peaks at 64.1 ppm, 73.5 ppm, 82.1 ppm and 104.5 ppm, which are in excellent agreement with the peaks observed in the difference spectrum shown in Fig. 2B. It is important to mention that although there is a peak at 73.5 ppm, it corresponds to a broad line ranging from ~70–77 ppm that can account for the two peaks observed in the difference spectra of Fig. 3B. Moreover, except for the absence of the signal at ~ 62 ppm (C6 carbon of cellulose domain 2), the predicted spectrum of the long T_1 component shows all the peaks with the chemical shifts expected for pure cellulose

samples (Falcoz-Vigne et al., 2017; Larsson et al., 1997; Foston, 2014).

The reduced intensity of the C6 carbon signal at ~62 ppm is easily explained considering the higher mobility expected for the hydroxymethyl groups in the less conformationally ordered domain 2 of cellulose which leads to fast T_1 relaxation. In other words, hydroxymethyl groups of cellulose reveal themselves in the spectrum as a short T_1 component. Therefore, we could successfully separate the signals arising from cellulose (long relaxation component) and hemicellulose plus C6 carbons (short relaxation component). As already discussed, based on the main chemical shifts, the hemicellulose signals can be attributed to xylan in two-fold ribbon-like conformation associated with the surface of cellulose (Simmons et al., 2016).

The MCR procedure also allows to obtain the weight percentage of each component as a function of τ. Thus, it is possible by an ordinary exponential fitting, to estimate the concentration of each component at $\tau = 0$ (the full intensity), as well as the corresponding T_1 relaxation times. Those are given in Table 4 separately for each sample. Although it is clear that the weight percent of the short T_1 relaxation component is higher in the samples pretreated with NaOH 1% and the combined "alkali first" pretreated samples, it is important to stress that it cannot be associated only to the relative amount of xylan in the samples since a considerable part of the signals arises from C6 carbons of cellulose hydroxymethyl groups. However, it is rather consistent that the difference between the ssNMR spectra of the samples submitted to the combined "alkali first" and "acid first" pretreatments is the amount of xylan in two-fold ribbon-like conformation bound to the cellulose microfibril surface. As alluded to above, the T_1 relaxation times can also be obtained from the MCR analysis that provides intensity versus τ decay curves for each spectral component. The decay curves are shown in the Figs. S1 D and F and the T_1 values for the short T_1 component are given in Table 4. The T_1 relaxation time is considerably shorter for the sample pretreated "acid first". This may be a result of a less packed environment and higher conformational disorder of the molecules at the cellulose surface, favoring presence of the fast molecular motions that contribute to the reduction of T_1.

Finally, we should mention that we did not include the raw SCB and the samples pretreated only with diluted acid in the MCR analysis because these samples are too different of the alkali pretreated ones due to the higher amount of lignin, including an extra source of variation in the data matrix (high variability in the lignin signals). Since PCA, the base of MCR handling with variability, the inclusion of this samples forces the model to estimate an extra component (the lignin and associated signals specific of only acid treatment samples) which was not the main focus of our study.

To demonstrate this, in Fig. S1 of the Supplementary information, we included a comparison between the MCR analysis with and without the spectra of the sample submitted only to dilute acid pretreatment. The ^{13}C CPMAS spectra of the samples included in this analysis are shown in Fig. S2 A. Concerning the estimated spectra of the polysaccharides (Fig. 2 B) both procedures give the same results, proving the robustness of the proposed method, since even in the presence of an interferent (lignin), the results were essentially the same. However, if the spectra from dilute acid pretreatment samples were included in the MCR analysis, we observed a third (spurious) component which is identical to a typical lignin spectrum with some extra peaks that can be assigned to carbohydrates (Fig. S2 C). This might be associated with the fact that dilute acid pretreated samples, in addition to higher concentration of lignin, have higher content of carbohydrates. The latter carbohydrates presumably are solubilized during the combined treatment. Because the contents of carbohydrates and the lignin are higher in the diluted acid pretreated samples (and therefore are correlated), the MCR "puts" both of them in the same component. This indeed can be the basis of a method to separate the main spectral components of the ssNMR spectra using MCR. We are currently performing experiments and analyses to further validate to this procedure.

As already mentioned, the C4 carbon signal split accounts for the two distinct cellulose domains. Indeed, as shown previously (Dupree et al., 2019) each of these domains is composed by at least three subdomains due to different local conformations of the glucopyranosyl residues in the microfibril structure. The presence of these subdomains in our samples can be observed by the inhomogeneous line broadening of the C4 carbon signals in Fig. 2, but unfortunately it is not possible to separate the individual signals solely based on the 1D ^{13}C CPMAS spectra. To do so we built upon an early work of Wickholm, Larsson and Iversen (Wickholm et al., 1998) where the C4 signals at 80–88 ppm region was decomposed in different signals corresponding to the different subdomains. It is worth of notice that, despite the attribution of each subdomain signal to specific cellulose motifs (different crystal forms of internal cellulose, surface cellulose chains, paracrystalline and amorphous domains) has been reinterpreted with the newly proposed model for the cellulose microstructure (Dupree et al., 2019), the existence of subdomains associated to different conformations of the glucosyl residue still remains valid. Thus, as proposed by Wickholm and coworkers (Wickholm et al., 1998), we considered that the C4 signals of the cellulose ^{13}C CPMAS spectrum of domain 1 to be composed by three lorentzian lines at 89.5, 88.7 and 87.9 ppm and a gaussian line at 88.4 ppm while the domain 2 signals represent superposition of gaussian line shapes at 85.3 ppm, 84.5 ppm, 84.1 ppm and 83.2 ppm. Based on this model, we set up a strategy to check the consistency of our analysis and to estimate the relative amount of xylan in two-fold screw conformation in each sample. As justified before, the C4 carbon signals in the predicted spectra for the long T_1 component (Fig. S1 C) is likely to be only due to cellulose. Thus, we first fit the C4 signal region considering the aforementioned line positions and shapes for each sub-domain, allowing a maximum variation of 0.5 ppm in the line position to account for differences in our samples. The best fit is shown in Fig. S1 A. From this fit we obtained a set of line positions, widths and shapes which correspond to the cellulose in our samples. Then, we fit the ^{13}C CPMAS spectra of samples pretreated with "alkali first" and "acid first" using the obtained line shapes with position and widths fixed, i.e. only the line intensities were allowed to vary. Furthermore, we added a Gaussian line with a position fixed at 82.3 ppm to account for the xylan signal (based on the difference spectrum of Fig. 2 B and the predicted spectrum of the short T_1 component in Fig. 3C). The resulting fittings are shown in Fig. S1 B and C. Then, from the relative areas between the xylan signals and the total area of the cellulose signals we evaluated the percent fraction of two-fold screw xylan in each sample (Table 4). As one can see, about two times more two-fold screw xylan is retained in the sample pretreated with "alkali first" (16% ± 1%) as compared to "acid first" pretreatment (7% ± 1%). It is remarkable that the differences observed in the ^{13}C CPMAS spectra of the samples pretreated with "alkaline first" and "acid first" can be well explained only considering a different amount of cellulose sub-domains and xylan in two-fold conformation (highlighted as thicker lines in Fig. 3).

It is important to mention that the fractions of xylan in two-fold conformation given in Table 4 were computed with respect to the cellulose present in the respective samples. Taken into account chemical

Table 4
Content of short and long T_1 components estimated by MCR analysis of the CPT_1 spectra; Values of the short T_1 component (from MCR) and of the C6 (from Factor Analysis). The values of the long T_1 component are not shown because they are not reliable due to the short maximum τ value used in the dataset. The last column shows the fraction of two-fold xylan in the samples subjected to combined pretreatments as obtained by the fitting shown in Fig. 2.

Sample	Short T_1 (%)	Long T_1 (%)	T_1 Short (s)	T_1 C6[a] (s)	Fraction of two-fold xylan (%)
H_2SO_4 1% + NaOH 1%	25 ± 1	75 ± 1	0.8 ± 0.1	1.1 ± 0.1	7 ± 1
NaOH 1% + H_2SO_4 1%	33 ± 1	67 ± 1	1.6 ± 0.2	1.0 ± 0.2	16 ± 1

[a] T_1 C6: estimated from Factor Analysis after varimax rotation.

composition of the pretreated samples (Table 1) practically all xylan remining in the samples subjected to the combined "alkaline first" pretreatment is in two-fold ribbon-like flattened conformation characteristic of xylan bound to the surface of cellulose, whereas most of the xylan in "acid first" pretreated samples is in three-fold screw conformation which is found in xylan bound to lignin (about 60%). This is also consistent with the larger amount of lignin found in latter samples (Table 1).

It is worth mention that, despite the results show that the % of water in these interstitial spaces is higher in the "alkali first" as compared with the "acid first" pretreated samples, the enzymatic glucan conversion is less efficient in former samples. This indicated that the higher amount of two-fold xylan in the surface of the cellulose fibers is a more severe limiting factor to the efficiency of enzymatic hydrolysis than the water accessibility to the internal structures. Furthermore, the higher absorption of water within the inner interstitial spaces of the "alkali first" pretreated samples can be correlated to the coverage of the cellulose microfibers by the two-fold xylan leading to the increase in the hydrophilicity of the surface.

In summary, our ^{13}C CPMAS and PCA/MCR results provide evidences that the "acid first" combined pretreatment provides SCB samples with much smaller fraction of xylan associated with the surface of cellulose (two-fold conformation). Furthermore, the residual amorphous carbohydrates in the samples after "acid first" pretreatment have faster molecular dynamics (i.e. shorter T_1) than in the SCB samples after combined pretreatment with the basic pretreatment applied as the first step. This is consistent with the notion that acid pretreatment mostly depolymerize hemicellulose, whereas alkaline pretreatment provokes catalytical deconstruction and solubilization of lignin. It was recently shown that lignin forms strong electrostatic interactions with the polar motifs of xylan in three-fold conformation which is not associated with cellulose microfibrils (Kang et al., 2019). Consistently, chemical pretreatments that affect lignin, such as alkaline pretreatment, are likely to interfere mostly with the three-fold xylan, whereas acid-catalyzed pretreatments would preferentially hydrolyze xylan in two-fold screw conformation tightly associated with cellulose. Indeed, as already mentioned, the ^{13}C CPMAS spectra from the samples pretreated only with NaOH 1% show significant similarity with the spectra of the samples pretreated with "alkali first" which indicates importance of the first (NaOH) pretreatment step and a reduction in the efficiency of the second (H_2SO_4) pretreatment step. Finally, we also would like to point out that although the ^{13}C NMR measurements and the PCA/MCR procedures applied here are known, but, to the best of our knowledge, this is the first time that MCR is used to identify a source of variation induced by a NMR pulse sequence, obtaining molecular dynamic properties of cellulose and xylan in the intact biomass samples. This procedure holds a significant promise given a fact that NMR is well known by its capability of revealing different physical chemical information in the spectra using specific pulse sequences (Falcoz-Vigne et al., 2017; Larsson et al., 1997; Foston, 2014). To find out how the observed differences in chemical composition and physical structure of pretreated SCB samples impacted their enzymatic degradation, we conducted their hydrolysis using commercial enzymes Accellerase 1500 (Genencor, Rochester, NY, USA).

3.5. Enzymatic hydrolysis of the SCB samples

Experimentally measured enzymatic hydrolysis yields and rates were considerably different for the pretreated SCB samples (Fig. 4). As expected (Maeda et al., 2011; Santo et al., 2018; Brar et al., 2020), efficiency of cellulose enzymatic hydrolysis of raw SCB samples was quite low (less than 20%) in all studied time intervals (Fig. 4).

From the pretreated samples, the lowest glucan conversion was observed for the single-step acid-pretreated samples (Fig. 4 A), indicating that the chosen enzymatic dose was not sufficient to hydrolyze large fraction of the cellulose after diluted-acid pretreatment only. Although being superior to raw SCB samples, even after 72 h of hydrolysis only just over 30% of the cellulose has been enzymatically converted into glucose in the samples pretreated solely with H_2SO_4 (Fig. 4 A). Notably, a large fraction of lignin remained in the acid-pretreated samples under experimental conditions employed in this work (Table 1). Studies of dilute acid pretreatment revealed that lignin tends to coalesce into aggregates, subjected to depolymerization and repolymerization reactions and precipitate at the surface of the pretreated biomass (Santo et al., 2018; Espirito Santo et al., 2019; Brar et al., 2020; Chiarello et al., 2019), which is consistent with the enlarged confocal microscopy autofluorescence spectra observed for the dilute acid pretreated SCB samples in our analyses. Lignin rearrangements, mainly characterized by its removal from the inner parts of the cell wall and redeposition on the surface, was observed for other lignocellulosic biomasses submitted to diluted acid (Brar et al., 2020; Chiarello et al., 2019; Selig et al., 2007). In addition, lignin fragments could interfere with cellulases causing their deactivation and unproductive binding to the lignin redeposited on the biomass surface (Qing et al., 2010). These effects taken together might explain observed low efficiency of cellulose enzymatic hydrolysis in single-step acid pretreated samples.

On the other hand, sodium hydroxide is one of the strongest base catalysts (Carvalheiro et al., 2009; da Cruz et al., 2012), and the efficiency of applied NaOH 1% pretreatment is evidenced by an elevated degree of glucan conversion (Fig. 4 A). After first 24 h the single-step alkaline pretreated SCB samples (NaOH 1%) had much higher cellulose enzymatic hydrolysis yield, indicating that lignin removal significantly improved access of cellulases to cellulose fraction. However, little further improvement was observed in the cellulose degradation of NaOH 1% pretreated sample within the following 48 h.

Combined pretreatments led to an enhanced release of glucose as a result of cellulose enzymatic degradation. Notably, the hydrolytic rates

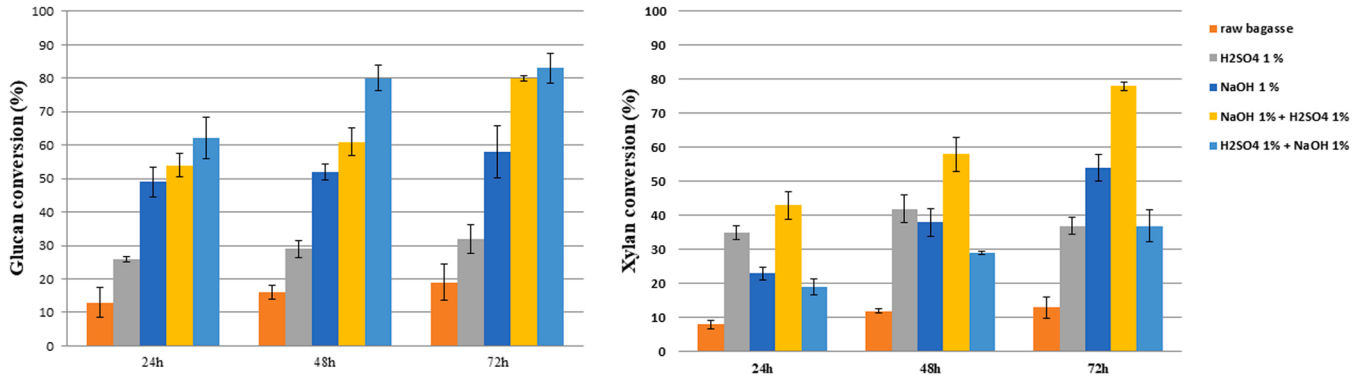

Fig. 4. Enzymatic hydrolysis yields based on A) glucan and B) xylan conversion after 24, 48 and 72 h. The error bars are standard deviations from the average values of triplicate measurements.

of "acid first" pretreated samples were significantly better, reaching 80% of cellulose depolymerization within the first 48 h (Fig. 4 A). Although "alkaline first" and "acid first" pretreatments both led to pretreated SCB samples providing glucan conversion yields close to (or even slightly higher than) 80% after 72 h of reaction time, the hydrolytic rates of the "alkaline first" combined pretreated samples were considerably slower as compared to SCB samples submitted to the "acid first" combined pretreatment (Fig. 4 A). One reason for that could be somewhat smaller content of glucan in the SCB samples submitted to "acid first" pretreatment (Table 1), which, at the same enzymatic loadings, may lead to the faster enzymatic degradation of cellulose. Another reason for the observed differences in the rates of enzymatic hydrolysis could be directly related to the dissimilar amount of xylan in two-fold conformation detected in the SCB samples which underwent "acid first" or "alkaline first" combined pretreatments. Although overall contents of xylan in the "acid first" and "alkaline first" pretreated samples were approximately the same (Table 1), fractions of the xylan in two-fold conformation after these two pretreatments were very different, being much higher in the "alkaline first" pretreated SCB samples (Table 4). Finally, taking into account chemical composition of the "alkali first" and "acid first" pretreated SCB samples (Table 1), after 72 h of enzymatic hydrolysis, total glucose yield from "alkaline first" pretreated samples was higher as compared to "acid first" pretreated SCB.

It was demonstrated that xylan in the plant cell wall can adopt plane, beta-sheet-like two-fold conformation when bound to the surface of cellulose fibers (Simmons et al., 2016; Dupree et al., 2019). It is also known that xylan and xylooligosacharides (XOS) bound to the surface of cellulose create physical barrier which impedes an access of cellulases to cellulose fiber and slow down enzymatic hydrolysis (Qing et al., 2010). Although ribbon-like conformation of a two-fold xylan mimics the one of crystalline cellulose and almost perfectly adopts within the active-side tunnel of exoglycanases, binding of XOS within the active side of exoglucanases occurs in out-of-register as compared to cellooligosaccharides (Momeni et al., 2015) which essentially prevents their hydrolysis and inhibits enzymatic activity of the later enzymes. Indeed, long XOS are strong inhibitors of exoglucanases (Baumann et al., 2011) which are the main monocomponents of the commercial fungal enzymatic mixtures (Payne et al., 2015). Although β-xylanases, β-xylosidases and also some endoglucanases (Pellegrini et al., 2015) have an elevated capacity to hydrolyze xylan and long XOS into xylose and short XOS thus alleviating exoglucanase inhibition by long XOS, this process takes time, particularly in the case of more crystalline and recalcitrant two-fold xylan strongly bound to the surface of cellulose microfibers. This can contribute to the slower enzymatic hydrolysis rates of the "alkaline-first" pretreated biomass samples as compared to "acid first" pretreated SCB.

This notion was further supported by the results of xylan hydrolysis (Fig. 4 B). Whereas only about 37% of xylan fraction in the combined "acid first" pretreated samples was slowly hydrolyzed after 72 h of enzymatic hydrolysis, up to 80% of xylan in "alkaline first" pretreated samples was steadily converted into xylose in a course of hydrolysis (Fig. 4 B). As alluded to above practically all xylan in the latter samples is bound to the surface of cellulose in two-fold screw conformation and its enzymatic depolymerization and removal provides an access of cellulases to cellulose thus promoting its hydrolysis and liberation of glucose and cellooligosaccharides. Notably, a rate of two-fold xylan conversion in "alkaline first" pretreated samples (Fig. 4 B) is correlated with the rate of cellulose enzymatic hydrolysis (Fig. 4 A). The same seems to be true for the "acid first" pretreated samples (Fig. 4 A and B). It is worth notice that only about 40% of xylan in these samples is in two-fold flattened conformation characteristic of xylan bound to cellulose. The rest is in three-fold screw helical conformation typical for lignin-bound xylan. It is tempting to speculate that xylan-active enzymes in the enzymatic preparate used in our experiments were more efficient in hydrolyzing cellulose-bound fraction of xylan leading to overall conversion close to 40% within 72 h of hydrolysis. The rest of the xylan, protected by bound lignin, was chiefly inaccessible to the enzymes and remained unhydrolyzed in the "acid first" samples (Fig. 4 B). Smaller fraction of cellulose-bound xylan in "acid first" samples could also explain faster hydrolysis of their cellulose fraction which was essentially completed within the first 48 h.

4. Conclusions

Our results reveal that an order of the same pretreatment steps during combined pretreatments of lignocellulosic biomass has a strong effect on the chemical composition and physical structure of these complex and heterogeneous lignocellulose materials. In particular, not only amounts of residual lignin and glucan in the pretreated lignocellulosic biomass which underwent the same alkaline and acid pretreatments but in different order were different, but also a quantity of xylan in two-fold conformation, strongly associated with crystalline cellulose, was two times higher in "alkaline first" pretreated SCB samples as compared to "acid first" pretreated lignocellulose. Practically all xylan in "alkali first" pretreated biomass is associated with crystalline cellulose, whereas 60% of xylan in "acid first" pretreated samples is bound to lignin. Moreover, the overall rates and yields of the enzymatic hydrolysis of the pretreated lignocellulosic biomass using combined pretreatments (both of cellulosic and hemicellulosic fractions) are affected by the order in which these pretreatments were applied. Our experimental data show that although cellulose-bound two-fold xylan slows down a rate of glucan conversion, the final yields both of glucose and, particularly, of xylose were higher for "alkaline first" pretreated SCB after 72 h of hydrolysis. The obtained results and applied analytical methods could be relevant for optimization and analysis of lignocellulosic biomass pretreatments in general.

CRediT authorship contribution statement

Melissa C. Espirito Santo: Data curation, Formal analysis, Investigation, Validation, Writing – original draft. **Force Tefo Thema:** Data curation, Formal analysis, Investigation, Validation, Writing – original draft, Writing – review & editing. **Vanessa O. Arnoldi Pellegrini**: Data curation, Formal analysis, Investigation, Validation, Writing – original draft, Writing – review & editing. **Aissata Ousmane Kane**: Data curation, Formal analysis, Investigation, Validation. **Francisco E.G. Guimaraes:** Formal analysis, Methodology. **Jefferson G Filgueiras:** Data curation, Formal analysis, Investigation, Validation, Writing – original draft. **Etelvino Henrique Novotny:** Data curation, Formal analysis, Investigation, Validation, Methodology, Writing – original draft, Writing – review & editing. **Eduardo R. deAzevedo:** Data curation, Formal analysis, Investigation, Validation, Methodology, Writing – original draft, Writing – review & editing. **Igor Polikarpov:** Conceptualization, Resources, Formal analysis, Investigation, Validation, Methodology, Supervision, Funding acquisition, Writing – original draft, Writing – review & editing.

Declaration of Competing Interest

The authors declare that they have no known competing financial interests or personal relationships that could have appeared to influence the work reported in this paper.

Acknowledgments

This work was supported by Fundação de Amparo à Pesquisa do Estado de São Paulo (FAPESP, Brazil) via grant 15/13684-0 and by Conselho Nacional de Desenvolvimento Científico e Tecnológico (CNPq, Brazil) via grant 303988/2016-9.

Appendix A. Supporting information

Supplementary data associated with this article can be found in the online version at doi:10.1016/j.indcrop.2022.114708.

References

Anon 2021. http://www.shinshu-u.ac.jp/faculty/engineering/chair/chem010/manual/accellerase1500_Dupont.pdf.

Baumann, M.J., Borch, K., Westh, P., 2011. Xylan oligosaccharides and cellobiohydrolase I (TrCel7A) interaction and effect on activity. Biotechnol. biofuels 4 (1), 45. https://doi.org/10.1186/1754-6834-4-45.

Bernardinelli, O.D., Lima, M.A., Rezende, C.A., Polikarpov, I., deAzevedo, E.R., 2015. Quantitative 13C MultiCP solid-state NMR as a tool for evaluation of cellulose crystallinity index measured directly inside sugarcane biomass. Biotechnol. biofuels 8 (1), 110. https://doi.org/10.1186/s13068-015-0292-1.

Borgia, G.C., Brown, R.J.S., Fantazzini, P., 1998. Uniform-penalty inversion of multiexponential decay data. J. Magn. Reson. 132 (1), 65–77. https://doi.org/10.1006/jmre.1998.1387.

Brar, K.K., Santo, M.C.E., Pellegrini, V.O., deAzevedo, E.R., Guimaraes, F.E., Polikarpov, I., Chadha, B.S., 2020. Enhanced hydrolysis of hydrothermally and autohydrolytically treated sugarcane bagasse and understanding the structural changes leading to improved saccharification. Biomass-.-. Bioenergy 139, 105639. https://doi.org/10.1016/j.biombioe.2020.105639.

Brewer, C.E., Chuang, V.J., Masiello, C.A., Gonnermann, H., Gao, X., Dugan, B., Driver, L. E., Panzacchi, P., Zygourakis, K., Davies, C.A., 2014. New approaches to measuring biochar density and porosity. Biomass-.-. Bioenerg. 66, 176–185. https://doi.org/10.1016/j.biombioe.2014.03.059.

Capitani, D., Di Tullio, V., Proietti, N., 2012. Nuclear magnetic resonance to characterize and monitor cultural heritage. Prog. Nucl. Magn. Reson. Spectrosc. 64, 29–69. https://doi.org/10.1016/j.pnmrs.2011.11.001.

Carvalheiro, F., Silva-Fernandes, T., Duarte, L.C., Gírio, F.M., 2009. Wheat straw autohydrolysis: process optimization and products characterization. Appl. Biochem. Biotechnol. 153 (1–3), 84–93. https://doi.org/10.1007/s12010-008-8448-0.

Chabbert, B., Terryn, C., Herbaut, M., Vaidya, A., Habrant, A., Païs, G., Donaldson, L., 2018. Fluorescence techniques can reveal cell wall organization and predict saccharification in pretreated wood biomass. Ind. Crops Prod. 123, 84–92. https://doi.org/10.1016/j.indcrop.2018.06.058.

Chiarello, L.M.A., Ramos, C.E., dos Santos, L.F., Silveira, M.H., Zaccaron, S., Schiehser, S., Santo, M.E., Guimarães, F.E.G., Azevedo, E.R., Polikarpov, I., Potthast, A., Ramos, L.P., 2019. Characterization of pretreated fractions and cellulosic ethanol production from steam-exploded *Eucalyptus urograndis*. Energy Fuels 34 (1), 535–545. https://doi.org/10.1021/acs.energyfuels.9b03405.

Coletta, V.C., Rezende, C.A., da Conceição, F.R., Polikarpov, I., Guimarães, F.E.G., 2013. Mapping the lignin distribution in pretreated sugarcane bagasse by confocal and fluorescence lifetime imaging microscopy. Biotechnol. biofuels 6 (1), 43. https://doi.org/10.1186/1754-6834-6-43.

da Cruz, S.H., Dien, B.S., Nichols, N.N., Saha, B.C., Cotta, M.A., 2012. Hydrothermal pretreatment of sugarcane bagasse using response surface methodology improves digestibility and ethanol production by SSF. J. Ind. Microbiol Biotechnol. 39 (3), 439–447. https://doi.org/10.1007/s10295-011-1051-3.

Dick-Pérez, M., Zhang, Y., Hayes, J., Salazar, A., Zabotina, O.A., Hong, M., 2011. Structure and interactions of plant cell-wall polysaccharides by two-and three-dimensional magic-angle-spinning solid-state NMR. Biochemistry 50 (6), 989–1000. https://doi.org/10.1021/bi101795q.

Driemeier, C., Mendes, F.M., Santucci, B.S., Pimenta, M.T., 2015. Cellulose co-crystallization and related phenomena occurring in hydrothermal treatment of sugarcane bagasse. Cellulose 22 (4), 2183–2195. https://doi.org/10.1007/s10570-015-0638-7.

Dupree, P., Terrett, O., Lyczakowski, J., Yu, L., Franks, W.T., Brown, S., Dupree, R., 2019. Molecular architecture of softwood revealed by solid state NMR. Nat. Commun. 10 (1), 1–11. https://doi.org/10.1038/s41467-019-12979-9.

Espirito Santo, M.C., Cardoso, E.B., Guimaraes, F.E.G., DeAzevedo, E.R., da Cunha, G.P., Novotny, E.H., Pellegrini, V.O.A., Chandel, A.K., Silveira, M.H.L., Polikarpov, I., 2019. Multifaceted characterization of sugarcane bagasse under different steam explosion severity conditions leading to distinct enzymatic hydrolysis yields. Ind. Crops Prod. 139, 111542 https://doi.org/10.1016/j.indcrop.2019.111542.

Espirito Santo, M.C., Fockink, D.H., Pellegrini, V.O.A., Guimaraes, F.E.G., deAzevedo, E. R., Ramos, L.P., Polikarpov, I., 2020. Physical techniques shed light on the differences in sugarcane bagasse structure subjected to steam explosion pretreatments at equivalent combined severity factors. Ind. Crops Prod. 158, 113003 https://doi.org/10.1016/j.indcrop.2020.113003.

Falcoz-Vigne, L., Ogawa, Y., Molina-Boisseau, S., Nishiyama, Y., Meyer, V., Petit-Conil, M., Mazeau, K., Heux, L., 2017. Quantification of a tightly adsorbed monolayer of xylan on cellulose surface. Cellulose 24 (9), 3725–3739. https://doi.org/10.1007/s10570-017-1401-z.

Fengel, D. & Wegener, G. (1984) Wood: Chemistry, Ultrastructure, Reactions. De Gruyter, Berlin.

Foston, M., 2014. Advances in solid-state NMR of cellulose. Curr. Opin. Biotechnol. 27, 176–184. https://doi.org/10.1016/j.copbio.2014.02.002.

Foston, M.B., Hubbell, C.A., Ragauskas, A.J., 2011. Cellulose isolation methodology for NMR analysis of cellulose ultrastructure. Materials 4 (11), 1985–2002. https://doi.org/10.3390/ma4111985.

Himmel, M.E., Ding, S.Y., Johnson, D.K., Adney, W.S., Nimlos, M.R., Brady, J.W., Foust, T.D., 2007. Biomass recalcitrance: engineering plants and enzymes for biofuels production. Science 315 (5813), 804–807. https://doi.org/10.1126/science.1137016.

Ilanidis, D., Stagge, S., Jönsson, L.J., Martín, C., 2021. Effects of operational conditions on auto-catalyzed and sulfuric-acid-catalyzed hydrothermal pretreatment of sugarcane bagasse at different severity factor. Ind. Crops Prod. 159, 113077 https://doi.org/10.1016/j.indcrop.2020.113077.

Kang, X., Kirui, A., Widanage, M.C.D., Mentink-Vigier, F., Cosgrove, D.J., Wang, T., 2019. Lignin-polysaccharide interactions in plant secondary cell walls revealed by solid-state NMR. Nat. Commun. 10 (1), 1–9. https://doi.org/10.1038/s41467-018-08252-0.

Kawai, T., Nakazawa, H., Ida, N., Okada, H., Tani, S., Sumitani, J., Kawaguchi, T., Ogasawara, W., Morikawa, Y., Kobayashi, Y., 2012. Analysis of the saccharification capability of high-functional cellulase JN11 for various pretreated biomasses through a comparison with commercially available counterparts. J. Ind. Microbiol Biotechnol. 39 (12), 1741–1749. https://doi.org/10.1007/s10295-012-1195-9.

Kim, J.S., Lee, Y.Y., Kim, T.H., 2016. A review on alkaline pretreatment technology for bioconversion of lignocellulosic biomass. Bioresour. Technol. 199, 42–48. https://doi.org/10.1016/j.biortech.2015.08.085.

Larsson, P.T., Wickholm, K., Iversen, T., 1997. A CP/MAS13C NMR investigation of molecular ordering in celluloses. Carbohydr. Res. 302 (1–2), 19–25. https://doi.org/10.1016/S0008-6215(97)00130-4.

Lloyd, J.A., Murton, K.D., Newman, R.H., Suckling, I.D., Vaidya, A.A., 2017. Careful selection of steaming and attrition conditions during thermo-mechanical pretreatment can increase enzymatic conversion of softwood. J. Chem. Technol. Biotechnol. 92, 238–244. https://doi.org/10.1002/jctb.4975.

Maeda, R.N., Serpa, V.I., Rocha, V.A.L., Mesquita, R.A.A., Santa Anna, L.M.M., De Castro, A.M., Driemeier, C.E., Pereira Jr., N., Polikarpov, I., 2011. Enzymatic hydrolysis of pretreated sugar cane bagasse using *Penicillium funiculosum* and *Trichoderma harzianum* cellulases. Process Biochem. 46 (5), 1196–1201. https://doi.org/10.1016/j.procbio.2011.01.022.

Meng, X., Ragauskas, A.J., 2014. Recent advances in understanding the role of cellulose accessibility in enzymatic hydrolysis of lignocellulosic substrates. Curr. Opin. Biotechnol. 27, 150–158. https://doi.org/10.1016/j.copbio.2014.01.014.

Momeni, M.H., Ubhayasekera, W., Sandgren, M., Ståhlberg, J., Hansson, H., 2015. Structural insights into the inhibition of cellobiohydrolase Cel7A by xylo-oligosaccharides. FEBS J. 282 (11), 2167–2177. https://doi.org/10.1111/febs.13265.

Monshi, A., Foroughi, M.R., Monshi, M.R., 2012. Modified Scherrer equation to estimate more accurately nano-crystallite size using XRD. World J. Nano Sci. Eng. 2 (3), 154–160. https://doi.org/10.4236/wjnse.2012.23020.

Mosier, N., Wyman, C., Dale B Elander, R., Lee, Y.Y., Holtzapple, M., Ladisch, Ma, 2005. Features of promising technologies for pretreatment of lignocellulosic biomass. Bioresour. Technol. 96, 673–686. https://doi.org/10.1016/j.biortech.2004.06.025.

Novotny, E.H., Hayes, M.H., Madari, B.E., Bonagamba, T.J., Azevedo, E.R.D., Souza, A. A., Song, G., Nogueira, C.M., Mangrich, A.S., 2009. Lessons from the Terra Preta de Índios of the Amazon region for the utilisation of charcoal for soil amendment. J. Braz. Chem. Soc. 20 (6), 1003–1010. https://doi.org/10.1590/S0103-50532009000600002.

Overend, R.P., Chornet, E., 1987. Fractionation of lignocellulosics by steam-aqueous pretreatments. Philos. Trans. R. Soc. Lond. Ser. A, Math. Phys. Sci. 321 (1561), 523–536. https://doi.org/10.1098/rsta.1987.0029.

Park, S., Baker, J.O., Himmel, M.E., Parilla, P.A., Johnson, D.K., 2010. Cellulose crystallinity index: measurement techniques and their impact on interpreting cellulase performance. Biotechnol. biofuels 3 (1), 10. https://doi.org/10.1186/1754-6834-3-10.

Park, Y.C., Kim, J.S., 2012. Comparison of various alkaline pretreatment methods of lignocellulosic biomass. Energy 47 (1), 31–35. https://doi.org/10.1016/j.energy.2012.08.010.

Payne, C.M., Knott, B.C., Mayes, H.B., Hansson, H., Himmel, M.E., Sandgren, M., Ståhlberg, J., Beckham, G.T., 2015. Fungal cellulases. Chem. Rev. 115 (3), 1308–1448. https://doi.org/10.1021/cr500351c.

Pellegrini, V.O., Serpa, V.I., Godoy, A.S., Camilo, C.M., Bernardes, A., Rezende, C.A., Pereira Jr., N., Cairo, J.P.L.F., Squina, F.M., Polikarpov, I., 2015. Recombinant Trichoderma harzianum endoglucanase I (Cel7B) is a highly acidic and promiscuous carbohydrate-active enzyme. Appl. Microbiol. Biotechnol. 99 (22), 9591–9604. https://doi.org/10.1007/s00253-015-6772-1.

Qing, Q., Yang, B., Wyman, C.E., 2010. Xylooligomers are strong inhibitors of cellulose hydrolysis by enzymes. Bioresour. Technol. 101 (24), 9624–9630. https://doi.org/10.1016/j.biortech.2010.06.137.

Ragauskas, A.J., Williams, C.K., Davison, B.H., Britovsek, G., Cairney, J., Eckert, C.A., Frederick Jr., W.J., Hallett, J.P., Leak, D.J., Liotta, C.L., Mielenz, J.R., Murphy, R., Templer, R., Tschaplinski, T., 2006. The path forward for biofuels and biomaterials. Science 311 (5760), 484–489. https://doi.org/10.1126/science.1114736.

Rezende, C.A., de Lima, M.A., Maziero, P., deAzevedo, E.R., Garcia, W., Polikarpov, I., 2011. Chemical and morphological characterization of sugarcane bagasse submitted to a delignification process for enhanced enzymatic digestibility. Biotechnol. Biofuels 4, 54. https://doi.org/10.1186/1754-6834-4-54.

Rocha, G.J.M., Martin, C., Soares, I.B., Maior, A.M.S., Baudel, H.M., de Abreu, C.A.M., 2011. Dilute mixed-acid pretreatment of sugarcane bagasse for ethanol production. Biomass-.-. Bioenerg. 35, 663–670. https://doi.org/10.1016/j.biombioe.2010.10.018.

Santo, M.E., Rezende, C.A., Bernardinelli, O.D., Pereira Jr., N., Curvelo, A.A., Guimarães, F.E., Polikarpov, I., 2018. Structural and compositional changes in sugarcane bagasse subjected to hydrothermal and organosolv pretreatments and

their impacts on enzymatic hydrolysis. Ind. Crops Prod. 113, 64–74. https://doi.org/10.1016/j.indcrop.2018.01.014.

Scherrer, P., 1912. Bestimmung der inneren Struktur und der Größe von Kolloidteilchen mittels Röntgenstrahlen. In Kolloidchemie Ein Lehrbuch. Springer, Berlin, Heidelberg, pp. 387–409. https://doi.org/10.1007/978-3-662-33915-2_7.

Segal, L.G.J.M.A., Creely, J.J., Martin, A.E., Conrad, C.M., 1959. An empirical method for estimating the degree of crystallinity of native cellulose using the X-ray diffractometer. Text. Res. J. 29 (10), 786–794. https://doi.org/10.1177/004051755902901003.

Selig, M.J., Viamajala, S., Decker, S.R., Tucker, M.P., Himmel, M.E., Vinzant, T.B., 2007. Deposition of lignin droplets produced during dilute acid pretreatment of maize stems retards enzymatic hydrolysis of cellulose. Biotechnol. Prog. 23 (6), 1333–1339. https://doi.org/10.1021/bp0702018.

Sigmund, G., Hüffer, T., Hofmann, T., Kah, M., 2017. Biochar total surface area and total pore volume determined by N_2 and CO_2 physisorption are strongly influenced by degassing temperature. Sci. Total Environ. 580, 770–775. https://doi.org/10.1016/j.scitotenv.2016.12.023.

Silveira, M.H.L., Morais, A.R.C., da Costa Lopes, A.M., Olekszyszen, D.N., Bogel-Łukasik, R., Andreaus, J., Pereira Ramos, L., 2015. Current pretreatment technologies for the development of cellulosic ethanol and biorefineries. ChemSusChem 8 (20), 3366–3390. https://doi.org/10.1002/cssc.201500282.

Simmons, T.J., Mortimer, J.C., Bernardinelli, O.D., Pöppler, A.C., Brown, S.P., Deazevedo, E.R., Dupree, R., Dupree, P., 2016. Folding of xylan onto cellulose fibrils in plant cell walls revealed by solid-state NMR. Nat. Commun. 7 (1), 1–9. https://doi.org/10.1038/ncomms13902.

Singh, T., Vaidya, A.A., Donaldson, L.A., Singh, A.P., 2016. Improvement in the enzymatic hydrolysis of biofuel substrate by a combined thermochemical and fungal pretreatment. Wood Sci. Technol. 50, 1003–1014. https://doi.org/10.1007/s00226-016-0838-9.

Suckling, I.D., Jack, M.W., Lloyd, J.A., Murton, K.D., Newman, R.H., Stuthridge, T.R., Torr, K.M., Vaidya, A.A., 2017. A mild thermomechanical process for the enzymatic conversion of radiata pine into fermentable sugars and lignin. Biotechnol. Biofuels 10, 61. https://doi.org/10.1186/s13068-017-0748-6.

Sun, Y.E., Cheng, J.J., 2005. Dilute acid pretreatment of rye straw and bermudagrass for ethanol production. Bioresour. Technol. 96 (14), 1599–1606. https://doi.org/10.1016/j.biortech.2004.12.022.

Takai-Yamashita, C., Sato, E., Fuji, M., 2020. NMR as a tool to characterize the aggregation structure of silica nanoparticles in a liquid. KONA Powder Part. J. 37, 233–243. https://doi.org/10.14356/kona.2020012.

Torchia, D.A., 1978. The measurement of proton-enhanced carbon-13 T1 values by a method which suppresses artifacts. J. Magn. Reson. 30, 613–616. https://doi.org/10.1016/0022-2364(78)90288-3.

Tsuchida, J.E., Rezende, C.A., de Oliveira-Silva, R., Lima, M.A., d'Eurydice, M.N., Polikarpov, I., Bonagamba, T.J., 2014. Nuclear magnetic resonance investigation of water accessibility in cellulose of pretreated sugarcane bagasse. Biotechnol. biofuels 7 (1), 127. https://doi.org/10.1186/s13068-014-0127-5.

Wickholm, K., Larsson, P.T., Iversen, T., 1998. Assignment of non-crystalline forms in cellulose I by CP/MAS 13C NMR spectroscopy. Carbohydr. Res. 312 (3), 123–129. https://doi.org/10.1016/S0008-6215(98)00236-5.

Yang, J., Kim, J.E., Lee, S.H., Yu, J.-H., Kim, K.H., 2017. Evaluation of commercial cellulase preparations for the efficient hydrolysis of hydrothermally pretreated empty fruit bunches. BioResources 12, 7834–7840.